Open-Loop Orientability of Objects on Actuator Arrays

Jonathan E. Luntz, William Messner, and Howie Choset
Department of Mechanical Engineering
Carnegie Mellon University
Pittsburgh, PA 15213
jl9f@cmu.edu, bmessner@cmu.edu, choset@cs.cmu.edu

Abstract

An actuator array is a form of distributed manipulation where an object being transported and manipulated rests on a large number of supporting actuators. On a discrete array employing an open-loop field, some size and shape objects may have unstable equilibria due to this discreteness. The functional relationship between object dimensions relative to array spacing and rotational stability is examined, and a map of this function is generated. The geometry behind this relationship is also examined, and analytical expressions for the boundaries between stable and unstable regions in the map are derived.

1 Introduction

An actuator array is a form of distributed manipulation where many small stationary elements (which we call cells) cooperate to manipulate larger objects. Current applications of actuator arrays range from microelectromechanical systems transporting pieces of silicon wafer to large-scale arrays of motorized wheels transporting cardboard boxes. In such applications, an object lies on a regular array as it is transported and oriented. Many cells support the object simultaneously, and as it moves, the set of supporting cells changes. While supporting the object, each cell is capable of providing a traction force on it, and the combined action of all the cells supporting the object determines the motion of the object.

Two modes of operation may be used: open-loop (passive) and closed-loop (active). In a passive mode, the action of the cells is pre-programmed and constant, and a "force field" is established in which the object moves. In an active mode, information about the object's motion is used to update the action of the cells. Such information may be obtained from local sensing at each cell or from some global sensor, such as a vision system, and in either case, real-time communication either to or between cells is generally necessary. Passive modes are useful for object positioning and orientation tasks with simple motions which don't require extreme precision, while active modes are generally useful for more precise motions or more complex motions involving multiple objects. The need for closed-loop control for precise motion in the context of discrete actuator arrays will be made clear in this paper. However, it is usually simpler and less expensive to implement an open-loop mode.

For an open-loop system, it is generally desirable to scale the actuator array so that very large numbers of cells support an object. This provides an approximately continuous medium on which the object can rest, giving smoother and more predictable motion. In the limit of very small cells placed closely together, the array does in fact become a continuous medium providing a true force field. On such fields, the motion of an object can be predicted analytically, particularly if the field is designed to be conservative, such that potential field theory may be used [4].

Unfortunately, it is usually impractical to construct a system with enough actuators to justify the continuous medium approximation. The manipulated objects must be supported by relatively smaller numbers of cells. This requires that the discrete nature of an actuator array be taken into account when designing open-loop fields and when predicting the motion of objects. In particular, when attempting to orient an object, the precision of orientation is limited by the cell resolution relative to the object size.

In this paper, we investigate the effect of discrete actuator arrays on the rotational stability of objects at translational equilibrium. Certain objects have unstable orientations which would otherwise be stable in the continuous field limit. An object at rotational equilibrium on a regular array can rotate some distance before it changes its set of supports. (We refer to the event where a cell changes its support state a *cell transition*, and the cell involved a *transitioning cell*.) The angle at which this transition occurs and which cell is involved in the transition is a function of the dimensions of the object. After the first cell transition, the torque on the object changes. The direction of the torque determines the local rotational stability of the equilibrium. This paper deals with the characterization of the functional relationship between object dimensions (particularly width and height of a rectangular object) and local rotational stability.

Section 2 describes prior work done by the authors and others on the analysis of actuator arrays. Section 3 examines the types of cell transitions and relates them to stability. A map is generated over varying sizes and shapes of objects showing stable and unstable regions. Section 4 examines the geometry behind the boundaries between stability regions in the map, and regenerates the map by analytically forming the boundaries. Section 5 relates the results to the use of open-loop control strategies.

2 Prior Work

Actuator arrays represent a recent development in robotic manipulation which derived ideas from other manipulation fields.

Böhringer, et. al. [2] adapted ideas from work in minimalistic sensorless manipulation [1, 3] and applied them to a micromechanical actuator array to manipulate very small objects. A continuous field assumption was used and mathematics were developed to "lift" the continuously distributed force field to a net single force and torque field acting on the object. A "squeeze" field was analyzed to orient objects where all the actuators on each side of an imaginary line dividing the array pushed toward the line. They showed that the squeeze field orients polygonal objects to one of a finite number of orientations. Kavraki [4] supplied further analysis of continuous field microactuator arrays using elliptical potential fields to bring any object to a single orientation. She used potential functions to predict stable configurations of objects.

In previous papers, the authors [5, 6, 7] examined the dynamics of an object carried by a macroscopic discrete actuator array called the Modular Distributed Manipulator System (MDMS) (or Virtual Vehicle). Each cell in this array contains an orthogonally mounted pair of motorized roller wheels whose combined motion provides a directable traction force to an object resting on top. By explicitly modeling all of the support and traction forces, the authors derived the piecewise constant dynamics of this system. The inversion of these dynamics generates a wheel velocity field which produces desired parcel dynamics with a single equilibrium position regardless of symmetry and cell resolution, and, under certain assumptions, a single orientation to the resolution of the cells.

One of these assumptions was called the "Positive Rotation Property". This is a stability property relating the size and shape of an object and the actuator array to the open-loop orientation stability of the object at translational equilibrium. The examination of this property motivated the work in this paper. The results of this work apply not only to the MDMS, but to other discrete actuator arrays acting under any of a class of fields which includes the fields used by Kavraki and Böhringer and Donald.

3 Local Rotational Stability of Objects

The discrete nature of actuator arrays not only limits stable orientations of an object to within cell resolution, it also causes some objects to have an unstable local rotational equilibrium while other objects of slightly different size or shape would have stable local rotational equilibria. To determine whether a particular object has a locally stable rotational equilibrium, it is necessary to examine the first cell transitions a parcel makes when it rotates about its equilibrium.

We will limit this examination to rectangular objects on symmetric *squeeze-like* fields on square-lattice arrays with idealized point supports. Examples of two such fields are shown in Figure 1. The following notation will be used to define a squeeze-like field. Assign each cell in the array an index and denote the set of indices $\mathcal{A}$. For $i \in \mathcal{A}$, $\vec{X}_i = (x_i, y_i)$ refers to the position of the ith cell, and $r_i = \sqrt{{x_i}^2 + {y_i}^2}$. $\mathcal{A}_{\mathrm{I}}$ refers to the set of indices for the cells which lie in the first quadrant $(x_i, y_i > 0)$, $\mathcal{A}_{\mathrm{II}}$ the second quadrant, and so on. Each cell i applies a vector force $\vec{f_i} = \left(f_{i_x}, f_{i_y}\right)$ in the plane to the object.

A squeeze-like field is defined such that for all $k \in \mathcal{A}$, $\operatorname{sign}\left(f_{k_y}\right) = -\operatorname{sign}(y_k)$ and either $\operatorname{sign}(f_{k_x}) = -\operatorname{sign}(x_k)$ or $f_{k_x} = 0$. Also, for all $i \in \mathcal{A}_{\mathrm{I}} \bigcup \mathcal{A}_{\mathrm{III}}$, the scalar cross product $\vec{X}_i \times \vec{f_i} < 0$ and for all $j \in \mathcal{A}_{\mathrm{II}} \bigcup \mathcal{A}_{\mathrm{IV}}$, $\vec{X}_j \times \vec{f_j} > 0$. In other words all cells push "towards" the origin, and first and third quadrant cells apply a clockwise moment about the origin while second and fourth quadrant cells apply a counterclockwise moment about the origin. A symmetric squeeze-like field is such that mirror symmetry exists

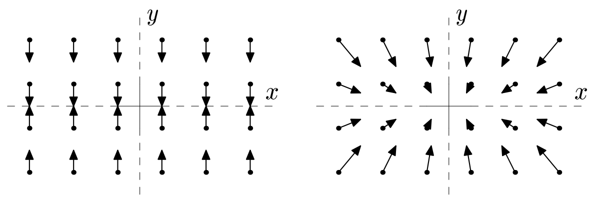

Figure 1: Two squeeze-like fields: A pure squeeze field (left) and an elliptical field (right). Note that the origin on in the left could be placed at any point on or between cells along the x-axis.

across both the x and y axes for both cell position and force. For example, for a cell $i \in \mathcal{A}_{\mathrm{I}}$ there is a cell $j \in \mathcal{A}_{\mathrm{IV}}$ such that $x_i = x_j$, $y_i = -y_j$, $f_{i_x} = f_{j_x}$, and $f_{i_y} = -f_{j_y}$. Both fields in Figure 1 have this property. We refer to the spacing of the square lattice as d.

We must properly place the origin of a squeeze-like field to maintain the "quadrant" nature and symmetry of the field. In general, the x-axis has a natural position, but the y-axis may have somewhat arbitrary placement (see Figure 1). Discretized versions of Böhringer's squeeze field[2] and Kavraki's elliptical potential field[4], as well as Luntz's computed field[7] are all squeeze-like, as are many other fields.

In general, squeeze-like fields transport objects to the origin (except for a pure squeeze field which has an arbitrary origin). After the object is brought to the origin, rotational equilibrium is reached when the object rotates to cover symmetric sets of cells in all quadrants. A rectangular object under a symmetric squeeze-like field with continuous field approximations will align itself such that its major axis coincides with the field's x-axis. Therefore, we will assume that the desired equilibrium orientation of a rectangular object on a discrete squeeze-like fields is such that its longer axis is aligned with the x-axis. To analyze the stability of the rotational equilibrium it is necessary to characterize the types of cell transitions.

3.1 Characterizing Transitions

Since the array and object are symmetric, from this point on we will speak of first and third quadrant cells as just first quadrant cells, and second and fourth quadrant cells as just fourth quadrant cells. We will also only analyze only positive (counter-clockwise) rotations of an object since negative rotations simply reverse the roles of the first and fourth quadrants.

The local stability of an object depends on the first cell transition that occurs as it rotates counter-clockwise. A rectangular object of width w and height h at orientation θ (relative to the desired orientation) will cover a set of supports $\mathcal{S}(\theta, w, h) \subset \mathcal{A}$. The angle where the set of supports first changes, $\alpha(w, h)$, is a function of object dimensions, and can be defined as $\alpha(w, h) > 0$ such that $\mathcal{S}(\theta, w, h) = \mathcal{S}(0, w, h)$ for $\theta \in (0, \alpha)$ and $\mathcal{S}(\alpha, w, h) \neq \mathcal{S}(0, w, h)$. Hereafter, we will drop the dependence on w and h for simplicity.

There are four possible ways in which the set of supports can change (see Figure 2):

Transition A The object rotates to touch a cell in the first quadrant not previously supporting the object (there will be only one such cell). We call this cell a newly covered first quadrant cell and label its index A. The angle at which this transition occurs is α_A. Define the set of first quadrant supports $\mathcal{S}_{\mathrm{I}}(\theta) = \mathcal{A}_{\mathrm{I}} \bigcap \mathcal{S}(\theta)$ (and similarly for the other quadrants). We can formally define $\alpha_A > 0$ such that $\mathcal{S}_{\mathrm{I}}(\theta) \subset \mathcal{S}_{\mathrm{I}}(0)$ for $\theta \in (0, \alpha_A)$ and $\mathcal{S}_{\mathrm{I}}(\alpha_A) \backslash \mathcal{S}_{\mathrm{I}}(0) = \{A\} \neq \emptyset$.

Transition B The object rotates to no longer touch a cell in the fourth quadrant which previously supported the object. We call this cell a newly uncovered fourth quadrant cell and label its index B. We can formally define $\alpha_B > 0$ such that $\mathcal{S}_{\mathrm{IV}}(\theta) \supset \mathcal{S}_{\mathrm{IV}}(0)$ for $\theta \in (0, \alpha_B)$ and $\mathcal{S}_{\mathrm{IV}}(0) \backslash \mathcal{S}_{\mathrm{IV}}(\alpha_B) = \{B\} \neq \emptyset$.

Transition C A cell is newly covered in the fourth quadrant. Label this cell C. The angle at which this transition occurs is α_C and is defined similarly to α_A.

Transition D A cell is newly uncovered in the first quadrant. Label this cell D. The angle at which this transition occurs is α_D and is defined similarly to α_B.

The first transition angle α therefore is equal to $\min(\alpha_A, \alpha_B, \alpha_C, \alpha_D)$. If $\alpha = \alpha_A$, then the newly covered cell applies a clockwise moment to the object while the rest of the supporting cells provide no net moment (since the object was previously in equilibrium). If $\alpha = \alpha_B$, then the counter-clockwise moment previously applied by the newly uncovered cell is removed and the net moment becomes clockwise. In either case there is a net negative torque which counteracts the positive rotation of the object, and the rotational equilibrium is locally stable. Conversely, $\alpha = \alpha_C$ and $\alpha = \alpha_D$ indicate an unstable local equilibrium. A special case occurs when two distinct types of transitions occur at the same angle. This indicates that such an object is on the boundary between stability and instability. Since α is a function of the object

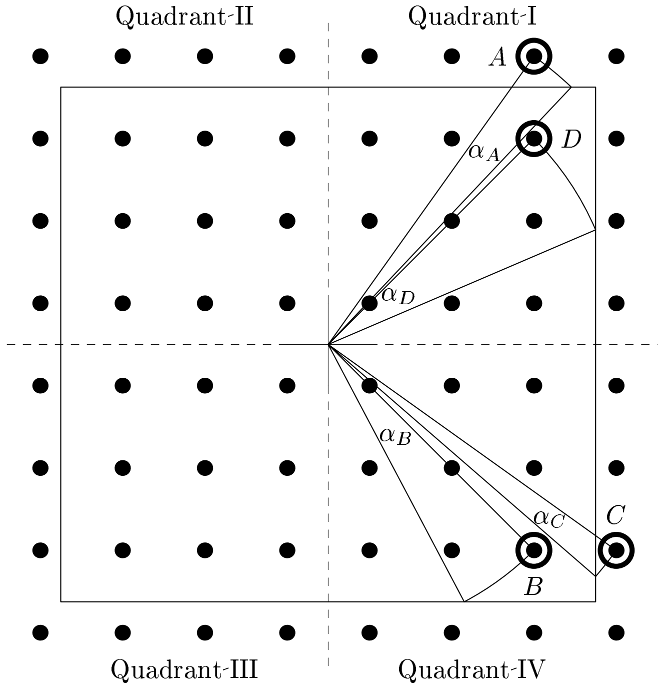

Figure 2: Four possible first transitions exist. Two are stabilizing (A and B) and two are destabilizing (C and D)

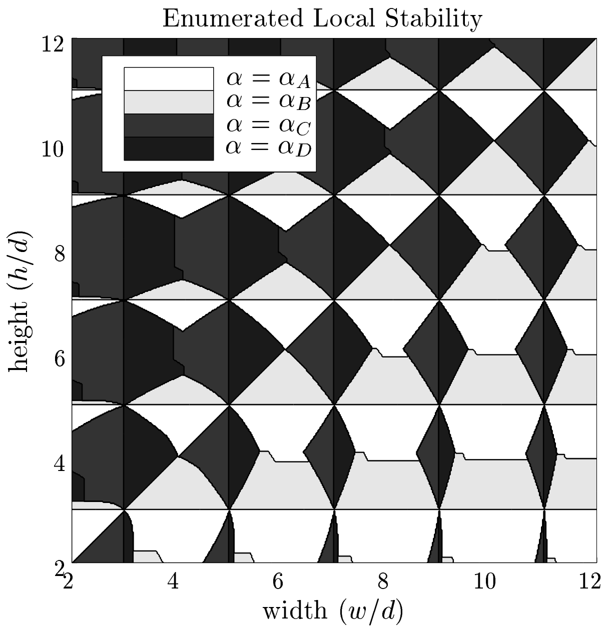

Figure 3: Local rotational stability of varying sizes of rectangular objects. Points colored in the lighter two shades of grey correspond to stable sized objects.

dimensions, local rotational stability is also a function of object dimensions. Therefore, we can generate a map of stability over the space of all possible object sizes w and h. To do this, we must first locate cells A, B, C, and D for a particular sized object.

3.2 Locating Transition Cells

In general, cells A, B, C, and D are the cells nearest the corner of the object which can be reached by the object. Cell D is the upper right-most cell under the object and cell B is the lower right-most cell under the object. There is no ambiguity in selecting these cells since the outermost cells under the object will always be the first cells to be newly uncovered.

Cells A and C are more difficult to locate. Cell A is is just above the object but may be just to the left of the upper right corner or one more cell to the left. The latter cell will be the transitioning cell if the former cell can not be reached by the corner of the object, *i.e.* it is not contained in the circle which circumscribes the object ($r_A > \sqrt{\frac{w^2}{4} + \frac{h^2}{4}}$). Similarly, cell C is just to the right of the object but may be just above the lower right corner or one more cell upward.

3.3 Computing The Stability Map

For a particular height and width of object, the angle to each of the first four possible transitions can be calculated now that these cells can be located. For example, the angle to transition A is

$$\alpha_A = \cos^{-1} \frac{h}{2r_A} - \cos^{-1} \frac{y_A}{r_A} \tag{1}$$

The other angles are computed similarly, and the smallest of which determines the stability. Figure 3 shows a map of the local rotational stability condition for all objects with width and height ranging between 2 and 12 cell spacings. In Figure 3, the area above the line $x = y$ corresponds to objects oriented with their long axis along the y axis rather than the x axis. We will ignore these “tall, narrow” objects, but it is interesting to note that their stability is exactly mirrored and opposite that of the “short, wide” objects.

In general, the stable regions (in the lower half of the figure) form vertical bands which narrow and widen regularly. The bands are centered on even (in terms of cell spacings) object widths, and the wide regions occur at odd object heights. Physically, odd heights mean the top and bottom sides of the object lie exactly on cells, causing stabilizing transitions types A and B to occur immediately. Even widths mean the left and right sides of the object lie exactly half-way between cells, causing destabilizing transition types C and D to occur at the largest possible rotation angle. Therefore, objects with even widths and odd heights tend to be the "most" stable. Conversely, objects with odd widths and even heights tend to be unstable. All of the local stability boundaries in the map in Figure 3 can be predicted geometrically and computed analytically. This is the topic of the next section.

4 Analytical Stability Boundaries

The stability boundaries in Figure 3 can be classified into three types: (i) *double transition* boundaries, where two transitions occur simultaneously, (ii) *corner transition* boundaries, where the corner of an object just touches a cell as the object rotates, and (iii) *edge transition* boundaries, where the side of an object just touches a cell as the object rotates.

4.1 Classifying Stability Boundaries

The four types of double transition boundaries can be generated by pairing an unstable and a stable first cell transition and are designated by the two transition types: AC, DB, DA, and BC. The first letter in each pair indicates which transition occurs first "inside" the boundary. The analytical expression for each of these boundaries (h as a function of w) is computed by equating the two corresponding transition angles (from Equation 1, for example). For example, boundary AC is expressed as

$$h = 2r_A \cos\left(\cos^{-1}\frac{y_A}{r_A} - \cos^{-1}\frac{x_C}{r_C} + \cos^{-1}\frac{w}{2r_C}\right) \tag{2}$$

This is an alternate expression for a skewed ellipse with the equation

$$h = -2r_A\sqrt{1-\left(\frac{w}{2r_C}\right)^2}\cos\phi + \frac{r_A}{r_C}w\sin\phi \tag{3}$$

where ϕ is the positive angle between the vectors from the origin to each of the transitioning cells. The algebra is omitted for space considerations. Figure 3 shows one such boundary extending down and to the left of the point $(7,5)$. Objects inside this boundary (narrower and taller) will be stable since they will make the A transition before the C transition.

Note that not all objects satisfying this equation will lie on an AC boundary. Small objects may not reach the cells used to compute the boundary, and large objects may hit other cells first. Only a small piece of the skewed ellipse is used to form the boundary, and intersections with other boundaries must be taken into account. The other double transition boundaries have expressions similar to Equation 3.

Corner transition boundaries occur when a cell lies exactly on the circle which circumscribes the object, such that the corner of the object just touches the cell. This contact may cause either a stabilizing or destabilizing moment depending on the dimensions of the object. The boundary consists of object sizes w and h such that $(w/2)^2 + (h/2)^2 = {r_R}^2$ for a particular cell R. Figure 3 shows such a boundary extending upward and to the left of the point $(7,5)$.

As the circular boundary passes through[1] the associated cell, the stable side of the boundary changes (see Figure 4). Below the cell (wider, shorter objects) the outside of the boundary corresponds to stability since the upper right corner of the object will encounter a first quadrant cell for larger objects. We refer to this portion of the boundary as an R_A boundary since a new A transition occurs outside the boundary. Above the cell (taller, narrower objects) the outside of the boundary corresponds to instability since the lower right corner of the object will encounter a fourth quadrant cell for larger objects. We refer to this portion of the boundary as an R_C boundary since a new C transition occurs outside the boundary. The R boundary has no effect on the region inside it since the cell to which the boundary corresponds is not touched by an object in this region.

Edge transition boundaries occur when the side of an object just touches a cell under the object when the object rotates. This would occur in Figure 2 if the arc drawn to cell D were tangent to the right side of the object. Such boundaries are vertical lines on the stability map where $w/2 = r_E$ for some cell E. Figure 3 shows edge transition boundaries extending upward from the bottom edge of the map. Objects wider than the vertical boundaries can not make the destabilizing D transition and hence are stable. Note that the bottom of the object generates horizontal boundaries which appear on the left edge of the map.

[1] When we say a boundary "passes through" a cell, it actually passes through a point with double the x and y coordinates of the cell. For example, the corner of an object of width 5 and height 3 will just touch a cell located at $(2.5, 1.5)$. To provide more physical understanding when plotting boundaries relative to cell locations, we will plot cell locations at double their coordinates and speak of boundaries passing through cells. (Alternatively, we could speak of object "half-widths" and heights rather than double cell locations.)

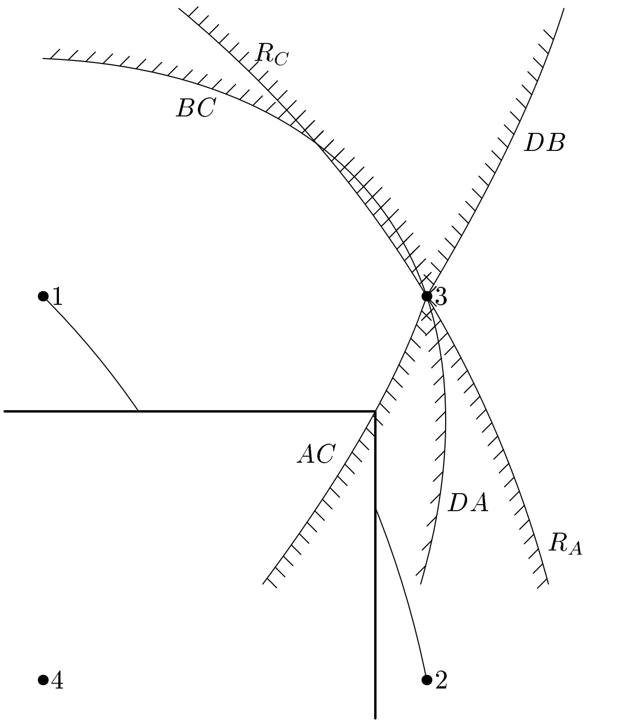

Figure 4: The local stability boundaries associated with a particular cell. The corner of an object on the AC boundary is drawn along with arcs to the cells with which it interacts. Note that for counter-clockwise rotations, the object actually interacts with the fourth quadrant right side cell, but it is equivalent to think of first quadrant cells with clockwise rotations as shown in the figure. Shading indicates the unstable side of each boundary. Since the R_A boundary only affects the region outside of it, it is not technically correct to mark the inside region unstable. It is marked here to indicate the outside region is stable.

4.2 Combining Boundaries

Some physical intuition is necessary to construct a complete diagram of the stability boundaries. First, we must index and instantiate all of the previously mentioned boundaries, and then we must draw them together accounting for intersecting boundaries and overlapping stability regions. Figure 4 shows each type of boundary (except an edge boundary) passing through the same cell (marked 3) to which they are indexed. This cell is located at $(5, 3)$ in Figure 3.

To instantiate the boundaries we must find the cells with which the object interacts to compute the boundary ellipse (from Equation 3, for example). Recall from Section 3.2 that cells B and D are easily located, but ambiguity exists in the location of cells A and C. For example, the upper-right corner of the object drawn in Figure 4 can rotate to touch cells 1 and 2 (mirrored from the fourth quadrant), as shown by the arcs extending to each cell. Since the arcs encompass the same angle, the object lies on the AC boundary. A small enough object on the AC boundary would not reach cell 2, and the boundary would be formed by the next cell in the column in which cell 2 lies. It is stated without proof that boundaries constructed by cells other than those adjacent to the corner of an object do not appear on the stability map. This is generally because the transition angle to non-adjacent cells is large enough that some other transition will occur first.

The AC boundary in Figure 4 passes through cell 3 since when the corner of the object lies on cell 3 at $\theta = 0$, its sides will coincide with cells 1 and 2, causing transitions with both these cells to occur immediately (and therefore simultaneously) as the object rotates. The AC boundary extends only below the cell since above the cell, the AC boundary becomes a DB boundary interacting with cell 3 just inside the corner. The cells with which we instantiate boundaries DB, DA, and BC similarly are adjacent to the cell through which the boundary passes, and these boundaries are also limited to one side of the cell. A corner (R) boundary is also shown in Figure 4 and is simply a circle passing through cell 3.

Combining the boundaries into a single coherent figure is a matter of determining which transitions occur in each region between boundaries. For example, in Figure 4, transition types A and B occur in the region between the DB and R_A boundaries. Therefore, this region is stable, as is the region between the DA and R_A boundaries where transition type A occurs. Similarly, the region between the AC and DA boundaries is unstable because C and D transitions occur. Even though the BC and R_C boundaries cross, the region above either (and both) of these boundaries is unstable since above either boundary, a C transition occurs. The upper region is unstable between these boundaries and the DB boundary since either C and D transitions occur. Finally, the region above the AC boundary and below both the BC and R_C boundaries is stable since A and B transitions occur.

When the boundaries associated with two cells intersect there are no ambiguities, and most of the entire diagram can be constructed in a straightforward manner. The only difficulty is the inclusion of the vertical edge transition boundaries. These boundaries are only significant for for very short ($h < 3d$) objects since the

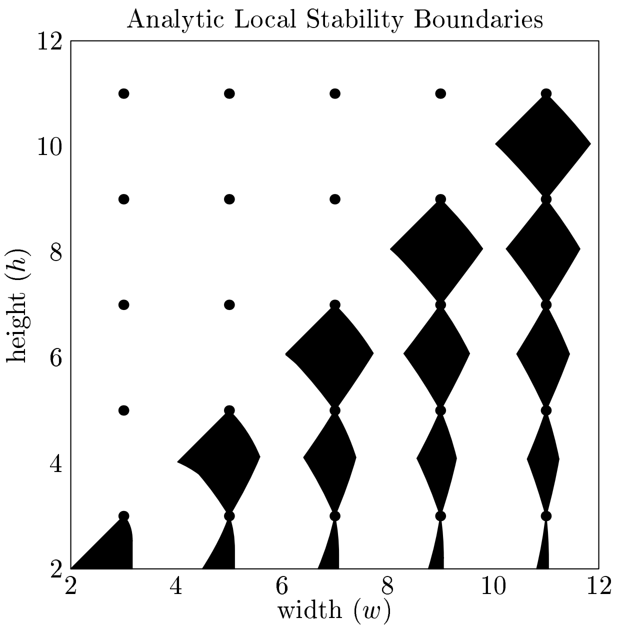

Figure 5: Analytically generated stability boundaries.

angle to the to the D cell (inside the upper left corner of the object) from the x-axis must be less than the angle to the B cell. Therefore, vertical (and horizontal) boundary lines will only appear along the bottom row (and left column) of the stability diagram.

Figure 5 contains a complete set of stability boundaries over the same range of object sizes used in Figure 3. Figure 5 was generated systematically in METAPOST by skewing and intersecting ellipses. Notice that Figure 5 is identical is shape to Figure 3.

5 Discussion and Conclusions

The results in this paper show that many objects experience local rotational instability on a discrete actuator array. Even very large objects may have unstable equilibria. This exposes a problem with the use of open-loop fields for orienting objects.

While a rotational equilibrium may be locally stable, there will generally be some angle, larger than the angle at which the unstable transition occurs, at which there is a net restoring torque. As an object rotates away from an unstable equilibrium, it will eventually find another equilibrium at this larger angle. This second equilibrium may be significantly larger than the angle to first transition, which is generally considered "cell resolution". Objects on the MDMS have been observed to find these stable secondary equilibria.

For increasingly larger objects, the angle to the first transition becomes smaller as does the angle to the secondary equilibrium. In the continuous limit the angle of the secondary equilibrium approaches zero even though the equilibrium at zero is technically unstable. Therefore, for very large objects or very dense arrays unstable local equilibria are not a problem.

This paper shows, however, that objects on moderately dense arrays cannot be oriented in open-loop with much precision. This suggests the use of closed-loop fields when any degree of rotational precision is required. Closed-loop fields can provide more accuracy with fewer cells, but require sensing and feedback increasing the complexity of the system.

References

[1] S. Akella, W. Huang, K.M. Lynch, and M.T. Mason. Sensorless parts feeding with a one joint robot. In *Proceedings. Workshop on the Algorithmic Fundamentals of Robotics*, 1996.

[2] K.F. Böhringer, B.R. Donald, R. Mihailovich, and N.C. MacDonald. A theory of manipulation and control for microfabricated actuator arrays. In *Proceedings. IEEE International Conference on Robotics and Automation*, 1994.

[3] K.Y. Goldberg. Orienting polygonal parts without sensors. *Algorithmica: Special Issue on Computational Robotics*, 10:201–225, August 1993.

[4] L. Kavraki. Part orientation with programmable vector fields: Two stable equilibria for most parts. In *Proceedings. IEEE International Conference on Robotics and Automation*, 1997.

[5] J. Luntz, W. Messner, and H. Choset. Parcel manipulation and dynamics with a distributed actuator array: The virtual vehicle. In *Proceedings. IEEE International Conference on Robotics and Automation*, 1997.

[6] J. Luntz, W. Messner, and H. Choset. Virtual vehicle: parcel manipulation and dynamics with a distributed actuator array. In *Proceedings of SPIE vol. 3201. Sensors and Controls for Advanced Manufacturing. International Symposium on Intelligent Systems and Advanced Maufacturing.*, 1997.

[7] J. Luntz, W. Messner, and H. Choset. Velocity Field Design on the Modular Distributed Manipulator System. In *Proceedings. Workshop on the Algorithmic Foundations of Robotics.*, 1998.